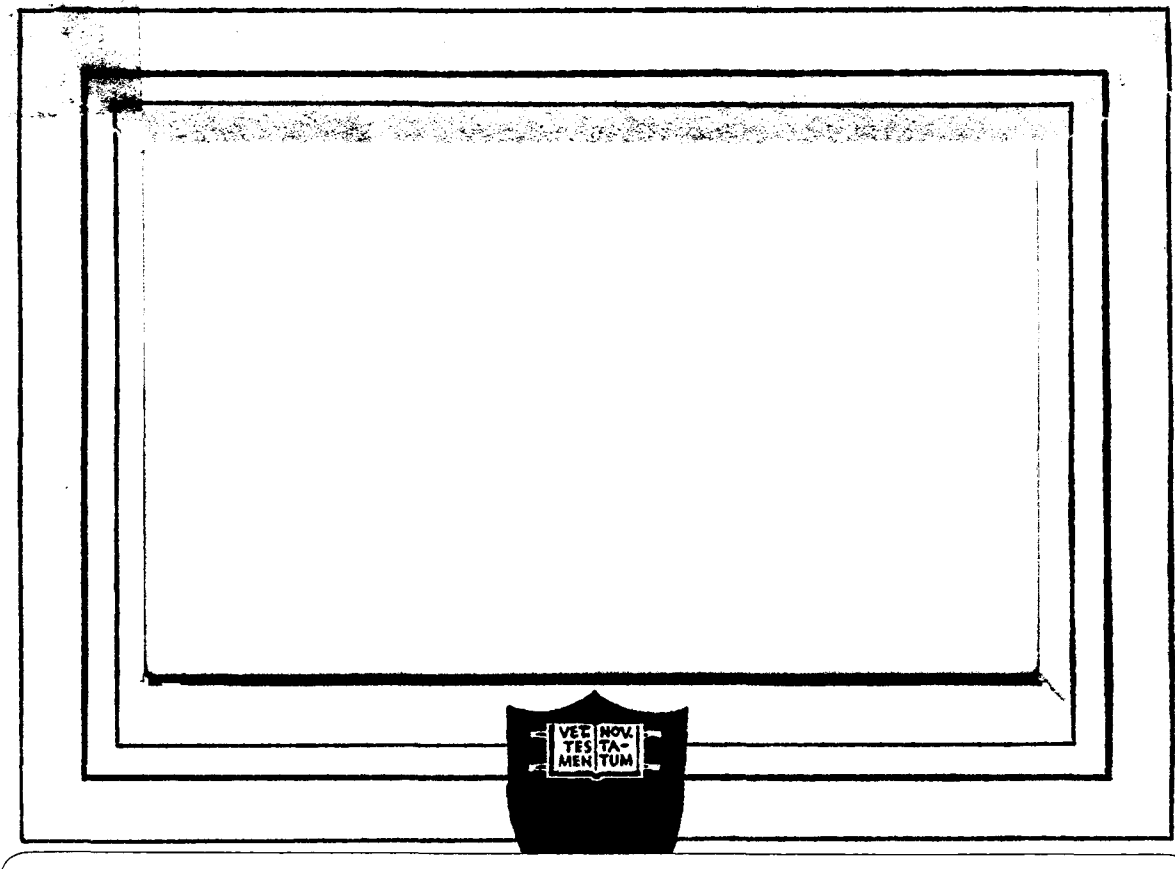

PRINCETON UNIVERSITY

DEPARTMENT OF AEROSPACE AND MECHANICAL SCIENCES

NONLINEAR ANALYSIS OF THE FLUTTER OF AN INFINITELY LONG PLATE

by

William Swan

AMS Report No. 845

August 1968

ACKNOWLEDGEMENT

The author would like to thank Professor E. H. Dowell for his guidance and advice. This work was supported by NASA Grant NGR31-001-059.

ABSTRACT

The flutter of an infinitely long plate in a high supersonic airstream is examined theoretically using Von Karman's nonlinear plate deflection equation and piston theory aerodynamics. By numerical methods the flutter is found to take the form of a traveling wave. To a close approximation the flutter motion can be described analytically. The case for flutter of loaded panels is also explored and analytic formulae developed. Solution in terms of more than one traveling wave is found to agree closely with the single wave behavior.

NOMENCLATURE

A_i, B_i	i^{th} mode amplitudes
a_i, b_i	non-dimensional amplitudes A_i/h and B_i/h
a	speed of sound
b	plate width
c	wave speed
D	plate stiffness $Eh^3/12(1-\nu^2)$
E	modulus of elasticity
h	plate thickness
ℓ	wavelength in x-direction
ℓ_i	i^{th} mode wavelength
M	mach number
N_x, N_y	in-plane stresses, x and y directions
$N_x^{(a)}$, $N_y^{(a)}$	applied in-plane stresses
$p-p_\infty$	perturbation pressure
q	dynamic pressure $\rho U^2/2$
$R_x = N_x^{(a)} b^2/D$	
$R_y = N_y^{(a)} b^2/D$	
t	time
U	air velocity
W	panel deflection in z-direction
W_T	W/h at a point
w_0	limit cycle modal amplitudes
x	lengthwise coordinate (stream wise)

y cross stream coordinate

z normal coordinate

i, j, k, m mode numbers

$\alpha_i = 2\pi x/\ell_i$

$\lambda = 2qb^3/D$

$\mu = \rho b/\rho_m h$ mass ratio

ν Poisson's Ratio ($\nu = .3$ was used)

ρ air density

ρ_m plate density

τ non-dimensional time $= \left(\frac{D}{\rho_m h b^4}\right)^{1/2}$

Φ plate stress function

ω non-dimensional frequency of flutter

$$\nabla^4( ) = \frac{\partial^4( )}{\partial x^4} + \frac{2\partial^4( )}{\partial x^2 \partial y^2} + \frac{\partial^4( )}{\partial y^4}$$

I. INTRODUCTION

Considered herein is the response of an infinitely long plate exposed to a length wise airflow and subjected to an initial disturbance. Motivation for the analysis came from Dowell's [4] discovery that the flutter of plates with high length to width ratios was dominated by modes too high to be conveniently examined by finite plate approaches. The analysis presented here would be valid for plates with length to width ratios above, say, ten if the effects of the ends become negligible as the plate length increases.

All analysis and terminology are derived from Dowell [4], whose major sources were Bolotin [1] and Librescu [6]. Dugundji [5] has investigated the linear case.

II. PROBLEM GEOMETRY

Consider a thin plate, pinned at both side edges and very long, subjected to a lengthwise air flow over the top surface (Fig. 1). Linear plate deflection theory predicts that, above a certain air flow velocity, any disturbance of the plate will become an exponentially growing oscillation. Finite plate analysis using Von Karman's nonlinear deflection equations shows that disturbances reach a steady state and the plate oscillates (flutters) indefinitely. Linear treatment of the aerodynamic forces is satisfactory for Mach numbers between 1.5 and 5. Finite plate analysis using Von Karman's plate deflection equations and piston theory (linear) aerodynamics has produced satisfactory agreement with experimental data (Dowell [2]).

III. LINEAR ANALYSIS

Linear analysis of this problem has been carried out by Dugundji [5]. Linear analysis predicts the flutter boundary, but describes all disturbances as decaying or growing exponentially. A review of the linear analysis follows.

Consider a simply supported infinitely long plate of width b and thickness h (Fig. 1). The plate is initially at rest, flat, and unstretched. An airstream passes over the upper surface. If the plate is given an initial disturbance, three linear effects are important in describing the motion. They are: inertial forces, aerodynamic forces, and the plate's resistance to bending. The deflection is described in terms of a travelling wave of the general form

$$W(x, y, t) = \sum_n \sum_m \cos \frac{m\pi y}{b} \left[A_n(t) \cos \frac{2\pi x}{\ell_n} + B_n(t) \sin \frac{2\pi x}{\ell_n}\right]$$

Only the first spanwise mode (m = 1) need be retained. For the linear case none of the modes are coupled, therefore each wavelength ℓ_n may be examined separately. Thus the wave form becomes

$$W = \cos \frac{\pi y}{b} \left[A \cos \frac{2\pi y}{\ell} + B \sin \frac{2\pi y}{\ell}\right] \tag{1}$$

The equation governing the motion is

$$\rho_m h \frac{\partial^2 W}{\partial t^2} = D\nabla^4 W - (p - p_\infty) \tag{2}$$

Using piston theory aerodynamics the aerodynamic forces are [2]

$$p - p_\infty = \frac{2q}{M} \frac{\partial W}{\partial x} + \frac{2q}{M} \frac{1}{U} \frac{\partial W}{\partial t} \tag{3}$$

Solution is by Galerkin's method. The deflection W is substituted from (1) into equation (2). The resulting equation is multiplied by

each of the mode shapes, cos ($\pi y/b$) cos ($2\pi x/1$) and cos ($\pi y/b$) sin ($2\pi x/1$). The two equations are then integrated over the panel width and n wavelengths producing the non-dimensionalized results below:

$$\frac{\partial^2 a_1}{\partial \tau^2} = -2\pi \frac{b}{\ell} \lambda b_1 - \sqrt{\lambda\mu} \frac{\partial a_1}{\partial \tau} - \pi^4 (4 \frac{b^2}{\ell^2} + 1) a_1$$

$$\frac{\partial^2 b_1}{\partial \tau^2} = 2\pi \frac{b}{\ell} \lambda a_1 - \sqrt{\lambda\mu} \frac{\partial a_1}{\partial \tau} - \pi^4 (4 \frac{b^2}{\ell^2} + 1) b_1 \qquad (4)$$

Note (4) is independent of n.

If we assume $a_1 = a_0 e^{i\omega\tau}$ and $b_1 = b_0 e^{i\omega\tau}$, then the condition for neutral stability is that ω be a pure real number. This condition predicts a flutter boundary of

$$\lambda = \frac{\ell^2}{b^2} \frac{\pi^2}{4} (4 \frac{b^2}{\ell^2} + 1)^2 \mu \qquad (5)$$

Thus the point at which a plate first flutters is expressed in terms of a relationship between the aerodynamic loading λ and the mass ratio μ. Flutter occurs at the lowest value of λ for a wavelength of twice the panel width, as can be seen by minimizing equation (5) with respect to ℓ/b and obtaining the critical values.

$$\lambda_{cr} = 4\pi^2 \mu$$

$$(\ell/b)_{cr} = 2$$

IV. NONLINEAR ANALYSIS

The nonlinear equation takes into account the stresses in the plate due to its being stretched like a membrane. Membrane stresses in plates are significant for deflections on the order of one plate thickness. The nonlinear equation is [4].

$$\rho_m h \frac{\partial^2 W}{\partial t^2} = \nabla^4 W - (p-p_\infty) + \frac{\partial^2 \Phi}{\partial x^2}\frac{\partial^2 W}{\partial y^2} + \frac{\partial^2 \Phi}{\partial x^2}\frac{\partial^2 W}{\partial x^2} - 2\frac{\partial^2 \Phi}{\partial x \partial y}\frac{\partial^2 W}{\partial x \partial y} \quad (6)$$

Where Φ is the stress potential function for the plate and obtained from

$$\frac{\nabla^4 \Phi}{Eh} = \left(\frac{\partial^2 W}{\partial x \partial y}\right)^2 - \left(\frac{\partial^2 W}{\partial x^2}\right)\left(\frac{\partial^2 W}{\partial y^2}\right) \quad (7)$$

If W from equation (1) is substituted into (7)

$$\frac{\nabla^4 \Phi}{Eh} = -\frac{2\pi^4}{\ell^2 b^2}\left[(A^2-B^2)\cos\frac{4\pi x}{\ell} + 2AB\sin\frac{4\pi x}{\ell} + (A^2+B^2)\cos\frac{2\pi y}{b}\right] \quad (8)$$

Assuming that the particular solution Φ_p is of the form

$$\Phi_p = T\cos\frac{4\pi x}{\ell} + Q\sin\frac{4\pi x}{\ell} + R\cos\frac{2\pi y}{\ell}$$

then substituting Φ_p into equation 7 and equating coefficients

$$T = -\frac{Eh}{128}\frac{\ell^2}{b^2}(A^2-B^2)$$

$$Q = -\frac{Eh}{84}\frac{\ell^2}{b^2}AB$$

$$R = -\frac{Eh}{8}\frac{b^2}{\ell^2}(A^2+B^2) \quad (9)$$

We assume for the homogeneous solution Φ_h the simplest form that will maintain any value of stress

$$\Phi_h = \bar{N}_y \frac{x^2}{2} + \bar{N}_x \frac{y^2}{2} + \bar{N}_{xy} xy \tag{10}$$

By the definition of a stress function the stresses in the plate are

$$N_x = \frac{\partial^2 \Phi}{\partial y^2} \ , \ N_y = \frac{\partial^2 \Phi}{\partial x^2}$$

The strains in the plate then are

$$\frac{\partial u}{\partial x} = \frac{1}{Eh} (N_x - \gamma N_y) - \frac{1}{2} \left(\frac{\partial W}{\partial x}\right)^2$$

$$\frac{\partial u}{\partial y} = \frac{1}{Eh} (N_y - \gamma N_x) - \frac{1}{2} \left(\frac{\partial W}{\partial x}\right)^2 \tag{11}$$

As boundary conditions we ask that there be no net inplane stretching over the width and n wavelengths:

$$\int_{-\frac{b}{2}}^{\frac{b}{2}} \int_{-\frac{n\ell}{2}}^{\frac{n\ell}{2}} \frac{\partial v}{\partial y} \, dxdy = 0 \quad \int_{-\frac{b}{2}}^{\frac{b}{2}} \int_{-\frac{n\ell}{2}}^{\frac{n\ell}{2}} \frac{\partial u}{\partial x} \, dxdy = 0 \tag{12}$$

Applying these conditions

$$\bar{N}_y = (A^2 + B^2) \frac{Eh}{1-\gamma^2} \left(\frac{\gamma\pi^2}{8b^2} + \frac{\pi^2}{2b^2}\right)$$

$$\bar{N}_x = (A^2 + B^2) \frac{Eh}{1-\gamma^2} \left(\frac{\pi^2}{8b^2} + \frac{\gamma\pi^2}{2\ell^2}\right) \tag{13}$$

$\bar{N}_{xy}$ is assumed to be zero, implying no resistance to in-plane shears. Note that these results are independent of n.

Equation (6) can now be expressed in terms of W. Applying Galerkin's method in the same manner as in the linear case, the equations become (in non-dimensional form):

$$\frac{\partial^2 a_1}{\partial \tau^2} = -2\pi \frac{b}{\ell} \lambda b_1 - \sqrt{\lambda\mu} \frac{\partial a_1}{\partial \tau} - \pi^4 (4 \frac{b^2}{\ell^2} + 1)^2 a_1 + E_4 a_1 (a_1^2 + b_1^2)$$

$$\frac{\partial^2 b_1}{\partial \tau^2} = 2\pi \frac{b}{\ell} \lambda a_1 - \sqrt{\lambda\mu} \frac{\partial b_1}{\partial \tau} - \pi^4 (4 \frac{b^2}{\ell^2} + 1)^2 b_1 + E_4 b_1 (a_1^2 + b_1^2)$$

where $$E_4 = -12\pi^4 (2 \frac{b^4}{\ell^4} + \nu \frac{b^2}{\ell^2} + \frac{1}{8}) - 12\pi^4 (1-\nu^2) \frac{b^4}{\ell^4} - \frac{3\pi^4}{4} (1-\nu^2) \quad (14)$$

The deflection $W = W(x, y, \tau; \lambda, \mu, \ell/b)$. Numerical solutions were obtained by integration of equations (14) on a digital computer.

V. SOLUTIONS AND RESULTS

Approximate Analytical Solution

Numerical integration of equation (14) produces a traveling wave form (Fig. 2). If the deflection is assumed to be a traveling wave, the limit cycle amplitude and frequency can be predicted analytically. We assume a time history of the form $a_1 = a_0 \cos \omega\tau$ and $b_1 = b_0 \sin \omega\tau$. Substituting into (14) and again applying Galerkin's method by multiplying the equations by cos $\omega\tau$ and sin $\omega\tau$ and integrating over a period, we obtain four equations in three unknowns ω, a_0, and b_0. However two pairs of equations are symmetrical in a_0 and b_0. If $a_0 = b_0 = w_0$, we get two equations in w_0 and ω. These reduce to

$$\omega = 2\pi \frac{b}{\ell}\sqrt{\frac{\lambda}{\mu}} \tag{15a}$$

$$w_0 = \left(\frac{\omega^2 - \pi^4(4\, b^2/\ell^2 + 1)^2}{E_4}\right)^{1/2} \tag{15b}$$

Using (12), w_0 may be written

$$w_0 = \left(\frac{4\pi^2 \frac{b^2}{\ell^2}\frac{\lambda}{\mu} - \pi^4(4\frac{b^2}{\ell^2} + 1)}{E_4}\right)^{1/2} \tag{16}$$

Numerical Solution

Equations (14) were step wise integrated under IBM 360 Fortran IV. One hundred steps per cycle of oscillation generally gave satisfactory accuracy. The limit cycle was usually reached in under one minute of computation. Longer times were necessary for low values of μ or λ/μ.

The analytic solution predicted the limit cycles obtained numerically well within the accuracy of the numerical data. Figure 3 shows the peak

of the oscillations approaching the theoretical asymptote with time. For practical applications μ's between .1 and .01 are of interest. While numerical results for $\mu = .1$ and $\mu = 1.$ corresponded exactly, numerical results for $\mu = .01$ and $\mu = .001$ fell consistantly 5% and 15% short of the analytically predicted amplitudes. Thus for mass ratios below .01, the analytical formulae do not produce good results. However, computation times for $\mu = .001$ are almost impossibly long so the analytical prediction may still be the most desirable method.

Discussion of Results

The results of the above analysis are presented in a series of graphs.

The dependence of the limit cycle deflection w_0 on the chosen ℓ/b is presented in figure 4. Notice the symmetry about $\ell/b = 2$. $\ell/b = 2$ is the critical point as was shown previously, but the maxima are not sharp. Figure 5 illustrates the dependences of the limit cycle amplitude upon a linear relationship between λ and $\mu(\lambda/\mu = \text{constant})$. An ℓ/b of two was used for all points, as suggested by figure 4.

The dependence of the limit cycle amplitude on λ/μ is also expressed in figure 6. The solid curve coincides with the curve obtained analytically. The dashed curve is the numerical result for a μ of .01 and illustrates that the analytical approximation just begins to break down for this small μ. Figure 7 has been included to illustrate the dependence of w_0 on λ for a finite plate. The limit cycle is relatively independent of μ; the dependence is on λ and not on λ/μ, as for an infinite plate. The present results suggest that for larger length to width ratio plates μ will become as important as λ.

Comparison with Finite Length Plate

It can be immediately seen from equation (16) that deflections of infinitely long plates depend on the ratio λ/μ and not on λ or μ independently. Notice that the aerodynamic dependence is on velocity (U^2) rather than on dynamic pressure q. This functional relationship is in direct contrast with results obtained by Dowell [4] for finite plates. Limit cycle amplitudes for finite plates depend strongly on λ (corresponding to q) and only weakly on μ. However there is some indication that μ becomes more important as the length to width ratio increases.

For infinitely long plates, an ℓ/b of exactly two produces the greatest deflection for a given λ/μ. This result can be proven by differentiating equation (16) with respect to ℓ/b. $\ell/b = 2$ is the critical point. This result suggests that in the limiting case of long finite plates the flutter amplitude will no longer depend on the plate length.

VI. DISCUSSION OF AERODYNAMICS

The assumptions made to justify piston theory aerodynamics were reconsidered in light of the above results. Dowell [7] had previously compared piston theory and higher order aerodynamics for the linear study of infinitely long plates. Linear theory was valid for high supersonic mach numbers.

In most uses, piston theory is valid whenever $M^2 >> 1$. However, for a traveling wave the relevant parameter is the relative mach number $M_r = (U - c)/a$, where c is the wave speed. Thus for traveling waves the condition is $M^2(1 - c/U)^2 >> 1$. Dowell's work revealed that at the flutter boundary $1 - c/U = 0$. Nevertheless he discovered that for large M the piston theory was still an acceptable approximation of the more exact results.

In our case numerical data and analytical results both predicted that $1 - c/U = 0$ <u>throughout</u> the nonlinear flutter range. (See figure 8; the analytical and numerical approaches agreed with the same degree of accuracy in predicting frequencies as they did in predicting deflection.) The result can be demonstrated analytically:

By definition

$$\frac{c}{\ell} = \frac{\Omega}{2\pi}$$

where Ω is the dimensional frequency. Our analytical solution for the flutter frequency gave

$$\omega_f = 2\pi \frac{\ell}{b} \sqrt{\frac{\lambda}{\mu}}$$

where

$$\omega \equiv \left(\frac{\rho_m h \Omega^2 b^4}{D}\right)^{1/2}$$

Combining the above equations, one may show that

$$1 - \frac{c_f}{U} = 0$$

Thus the piston theory is neither more nor less applicable for nonlinear flutter regime that it was on the flutter boundary.

While this result suggests that the present analysis is accurate only for very high supersonic mach numbers, the results may have significance beyond their theoretically limited range. The motivation for infinite plate analysis is the desire for comparison with long finite plate approaches. For comparison both cases should employ the same aerodynamic theory. Piston theory aerodynamics is valid down to mach numbers of two for finite plates, therefore such aerodynamics are of interest down to mach numbers near two for infinite plates.

VII. IN-PLANE LOADING

Consideration was also given to a plate with initial in-plane loading both from the ends at infinity and from the sides. Timoshenko [6] has developed the static buckling modes and loads for such a simply supported plate. Compression from the ends at infinity results in a buckling into lengthwise waves of wavelength 2b and a half-wave in the spanwise direction. Compression from the sides results in buckling into a half-wave in the spanwise direction with no lengthwise height variations (infinite wavelength 1).

First consideration was given to compressions from the ends at infinity. The compression enters into Φ of equation (6) as an additive stress $N_x^{(a)}$:

$$\Phi = T \cos \frac{4\pi x}{\ell} + Q \sin \frac{4\pi x}{\ell} + R \cos \frac{2\pi y}{b} + \bar{N}_x \frac{y^2}{2} + \bar{N}_y \frac{x^2}{2} + N_x^{(a)} \frac{y^2}{2}$$

Solution proceeds exactly as before and a term $R_x = N_x^{(a)} b^2/D$ appears in equations (14), viz.

$$\frac{\partial^2 a_1}{\partial \tau^2} = -2\pi \frac{b}{\ell} \lambda b_1 - \sqrt{\lambda\mu} \frac{\partial a_1}{\partial \tau} - \pi^2 (4 \frac{b^2}{\ell^2} + 1)^2 + E_4 a_1 (a_1^2 + b_1^2) - R_x a_1 4\pi^2 \frac{b^2}{\ell^2}$$

$$\frac{\partial^2 b_1}{\partial \tau^2} = 2\pi \frac{b}{\ell} \lambda a_1 - \sqrt{\lambda\mu} \frac{\partial a_1}{\partial \tau} - \pi^2 (4 \frac{b^2}{\ell^2} + 1)^2 + E_4 b_1 (a_1^2 + b_1^2) - R_x b_1 4\pi^2 \frac{b^2}{\ell^2} \tag{17}$$

If we assume $a_1 = a_0 \cos \omega\tau$ and $b_1 = b_0 \sin \omega\tau$ as before, we obtain an analytic solution for w_0. Equation (15a) ω is not altered by the addition of in-plane stresses. w_0 becomes

$$w_0 = [(4\pi^2 \frac{b^2}{\ell^2} \frac{\lambda}{\mu} - \pi^2 (4 \frac{\ell^2}{b^2} + 1)^2 - R_x \pi^2 4 \frac{b^2}{\ell^2}) / E_4]^{1/2} \tag{18}$$

Thus the effect of R_x is very similar to that of λ/μ. Numerical solutions of equations (17) once again bear out the validity of the assumed time dependence and reveal a series of shifted w_0 vs. λ/μ curves for various R_x's (see figure 9). Once again there is some deviation at lower μ's. There is no change in the behavior near the Euler buckling load $R_x = -4\pi^2$. However as λ approaches zero, the frequency of the oscillation slows and the deflections approach the static position. The oscillation continues to "pop through" from one static position to the mirror image position. There is no detectable tendency to superimpose small oscillations on a single static equilibrium position.

Both the unloaded flutter phenomenon and the Euler buckling phenomenon have their maxima at $\ell/b = 2$. By differentiation of equation (15) we can prove that the combined case also has a critical ℓ/b of 2.

The case is not quite so simple for compression from the sides. If sideloads are applied to an infinitely long plate, buckling takes the form of a curved surface with no variation of deflection in the lengthwise direction. This means a deflection with an infinite ℓ/b. But for the unstressed case the ℓ/b for maximum deflection at flutter is 2. Analysis analogous to the procedure outlined for $N_x^{(a)}$ produces a deflection

$$w_0 = [(4\pi^2 \frac{b^2}{\ell^2} \frac{\lambda}{\mu} - \pi^4(4 \frac{b^2}{\ell^2} + 1) - R_x\pi^2)/E_4]^{1/2} \qquad (19)$$

Solving for the critical point

$$(\frac{\ell}{b})_{\text{critical}} = [\frac{R_xL/\pi^2+(R_x^2L^2/\pi^4+2JL\nu+J^2L^2/16+(R_x/\pi^2+1)16\nu^2+R_xJL\nu/\pi^2)^{1/2}}{16\nu + JL}]^{-1/2}$$

$$J = \frac{4}{\pi^2} \frac{\lambda}{\mu} \qquad L = 3 - \nu^2 \qquad (20)$$

The plot of deflection vs ℓ/b for constant R_x and λ/μ (Figure 10) demonstrates the nature of this critical value. The maxima is less definite than the maximas at $\ell/b = 2$ were (Fig. 4). Indeed any ℓ/b greater than the critical ℓ/b produces deflections very near the maximum value.

The critical value of ℓ/b is greater than two for R negative (compression) and less than two for R_y positive (see Figure 11). Note that equation (20) applies only up to the flutter boundary. When R_y is so negative that there is no flutter but only buckling, ℓ/b is infinite.

The deflection w_0 is plotted against λ/μ in Figure 12. The ℓ/b for maximum flutter was used to obtain w_0 at each point. Unlike the unstressed case (Figures 5 and 6) or the end-loaded case (Fig. 9) the critical values of ℓ/b are not a constant.

VIII. MULTI-MODE SOLUTION

For nonlinear oscillations, disturbances need not take the form of a single wavelength. In order to examine this possibility a deflection composed of several wavelengths

$$W = \cos \frac{\pi y}{b} \left[\sum_n A_n(t) \cos \frac{2\pi x}{\ell_n} + B_n(t) \sin \frac{2\pi x}{\ell_n} \right]$$

can be substituted in place of the single mode deflection shape employed above. Performing the operations as before we find that each mode is generally coupled with all other modes. For example, the mode associated with $\ell/b = 2$ interacts with the wave associated with $\ell/b = 7.15$! It should be noted that the limits of integration $n\ell/2$ must go to infinity so that there will be no residual terms due to conditions at the ends of the plate.

Analysis in terms of more than one mode can proceed more simply however on the assumption that only the first ($\ell/b = 2$) mode is initially disturbed. While this is admittedly a special case, it is relevant to finite plates where the spectrum of possible wavelengths is limited to submultiples of the plate length. Only terms like

$$\int_{-n\ell/2}^{n\ell/2} A_i A_j A_k \cos \alpha_i x \cos \alpha_j x \cos \alpha_k x \cos \alpha_m x \, dx$$

contribute to the m^{th} mode equation of motion. Examination of this cosine product reveals that the integral is zero unless α_m can be obtained from a sum or difference of α_i, α_j, and α_k. We shall consider the case

where only the mode associated with an $\alpha = \alpha_1$ is excited initially. Since only A_1 is non-zero, only the term with $i = j = k = 1$ is non-zero. Thus the only other mode excited is $\alpha_m = \alpha_i + \alpha_j + \alpha_k = 3\alpha_1$. By sums and differences these two modes interact to excite the modes associated with $5\alpha_1$, $7\alpha_1$, $9\alpha_1$, and so on. This means that if one wavelength is excited only a discrete spectrum of shorter wavelengths are of interest, i.e., those which are odd integer multiples of the basic wave number.

The details of the analysis are given in the appendix.

Discussion of Results

The multi-mode solution was undertaken for two reasons. First as a check on the accuracy of a single mode solution. And second, in order to indicate which modes would be important to include in a finite plate analysis.

The equations of motion for coupled modes (see appendix for derivation) were integrated on a digital computer. In order to bring computation times within the available time limits (on the order of 5 minutes per run), several sacrifices in accuracy were made. Rather than use one hundred steps per cycle, about seventy points per cycle were computed (based on shortest period mode). Furthermore, limit cycles were not approached so closely as had been the case for the single mode solution.

Numerical runs were made by exciting the first ($\ell/b = 2$) mode and examining the limit cycle composed of the first mode and one or two subharmonics (see figure 13).

Limit cycles were within 10% of the limit cycles achieved for the single mode case. This is within the error of the multi-mode data. We

can thus conclude that the single mode solution is fairly well converged for moderate λ/μ.

Modes in the stable region have a very small effect on the oscillations. The amplitude of the stable mode tended to be no more than 2% of the amplitude of the unstable mode. The addition of a third stable mode to two unstable modes produced no detectable change in the motion at all.

Higher order modes in the unstable region had a detectable but distinctly secondary effect. For a λ/μ of 200, the addition of a second ($\ell/b = .667$) mode reduced the limit cycle amplitude slightly. The second mode's amplitude was never above 3% of the limit cycle amplitude.

The choice of $\ell/b = 2$ is justified only for checking the convergence of a single mode infinitely long plate solution. In order to explore behavior similar to the action of long finite plates, an unstable ℓ/b of six was used as the first mode (see Figure 13). It was found that the second ($\ell/b = 2$) mode still dominated the phenomena and that the importance of the longer wavelength was less than the importance of shorter wavelengths. This justified the use of $\ell/b = 2$ as the first mode for most comparisons.

In order to explore behavior comparable to a long plate which is able to permit $\ell/b = 2$, a run was made with two ℓ/b's symmetrically arranged around $\ell/b = 2$ (see Figure 13). The limit cycle was about two-thirds of that for $\ell/b = 2$, indicating greater stiffness for the off modes. The mode associated with the longer wavelength tended to dominate the phenomena. The shorter wavelength mode was about 10% of the limit cycle amplitude. For equally unstable modes the system seems to prefer the lower frequency mode. But more work must be done before any conclusions can be reached.

Most runs were made at $\mu = .1$. However one run was made at $\mu = 1.$, and the results were essentially the same. The agreement of $\mu = .1$ and $\mu = 1.$ indicates that the same λ/μ relationship holds for the multi-mode solution as did for the single mode solution.

IX. CONCLUSION

The flutter of an infinitely long plate can be described analytically by assuming the deflections take the form of a traveling wave. Limit cycles are a function of λ/μ and ℓ/b, with the greatest deflections occurring at an ℓ/b of 2. A single mode is usually satisfactory for describing the motion. The effect of secondary modes is especially small if the secondary modes are stable.

BIBLIOGRAPHY

1. Bolotin, V. V.: Nonconservative Problems of the Theory of Elastic Stability (MacMillan Co., New York, 1963), pp. 274-312.

2. Dowell, E. H. and Voss, H. M.: "Theoretical and Experimental Panel Flutter Studies in the Mach Number Range 1.0 to 5.0." AIAA J., vol. 3, 2292-2304 (1965).

3. Dowell, E. H.: "Generalized Forces on a Flexible Plate Undergoing Transient Motion." Quart. Appl. Math., 24, 331-338 (1967).

4. Dowell, E. H.: "Nonlinear Oscillations of a Flutter Plate." AIAA J., 4, 1267-1275 (1966).

5. Dugundji, J.: "Theoretical Considerations of Panel Flutter at High Supersonic Mach Numbers." AIAA J., 4, 1257-1266 (1966).

6. Timoshenko, S. P. and Gere, J. M.: Theory of Plastic Stability. (Maple Press Co., York, Pa., 1961), 348-379.

7. Dowell, E. H.: "The Flutter of Very Low Aspect Ratio Panels." Massachusetts Inst. of Technology, ASRL, 112-2, AD 608702, AFOSR 69-1723 (1964).

FIGURES

APPENDIX: MULTI-MODE SOLUTION

If $$W = \cos\frac{\pi y}{b} \sum_i \left(A_i \cos\alpha_i x + B_i \sin\alpha_i x \right)$$

Then $$\Phi = \sum_i \sum_j \Big(S_{1ij} \cos\alpha_i x \cos\alpha_j x + S_{2ij} \cos\alpha_i x \sin\alpha_j x$$

$$+ S_{3ij} \sin\alpha_i x \cos\alpha_j x + S_{4ij} \sin\alpha_i x \sin\alpha_j x$$

$$+ \cos\frac{2\pi y}{b} \Big(C_{1ij} \cos\alpha_i x \cos\alpha_j x + C_{2ij} \cos\alpha_i x \sin\alpha_j x$$

$$+ C_{3ij} \sin\alpha_i x \cos\alpha_j x + C_{4ij} \sin\alpha_i x \sin\alpha_j x \Big) \Big)$$

$$+ \bar{N}_x \frac{y^2}{2} + \bar{N}_y \frac{x^2}{2} + \bar{N}_{xy}\, xy$$

WHERE

$$S_1 = \frac{(R_1 T_1 + R_2 T_4)}{R_1^2 - R_2^2} \qquad C_1 = \frac{R_5 Q_1 + R_6 Q_4}{R_5^2 - R_6^2}$$

$$S_2 = \frac{R_1 T_2 - R_2 T_3}{R_1^2 - R_2^2} \qquad C_2 = \frac{R_5 Q_2 - R_6 Q_3}{R_5^2 - R_6^2}$$

$$S_3 = \frac{R_1 T_3 - R_2 T_2}{R_1^2 - R_2^2} \qquad C_3 = \frac{R_5 Q_3 - R_6 Q_2}{R_5^2 - R_6^2}$$

$$S_4 = \frac{R_2 T_1 + R_1 T_4}{R_1^2 - R_2^2} \qquad C_4 = \frac{R_5 Q_4 + R_6 Q_1}{R_5^2 - R_6^2}$$

The second and third subscripts have been left off. R, T, and Q are defined by

$$R_{1ij} = \alpha_i^4 + 6\alpha_i^2\alpha_j^2 + \alpha_j^4 \qquad R_{2ij} = 4(\alpha_i^3\alpha_j + \alpha_i\alpha_j^3)$$

$$R_{5ij} = R_{1ij} + (\alpha_i^2+\alpha_j^2)\,8\pi^2/b^2 + 16\pi^4/b^4$$

$$R_{6ij} = R_{2ij} + \alpha_i^2\alpha_j^2\,16\pi^2/b^2$$

$$T_{1ij} = \frac{2\pi^4}{b^2}\left(\frac{B_iB_j}{l_il_j} - \frac{A_iA_j}{l_i^2}\right)Eh \qquad Q_{1ij} = -\frac{2\pi^4}{b^2}\left(\frac{B_iB_j}{l_il_j} + \frac{A_iA_j}{l_i^2}\right)Eh$$

$$T_{2ij} = -\frac{2\pi^4}{b^2}\left(\frac{B_iA_j}{l_il_j} + \frac{A_iB_j}{l_i^2}\right)Eh \qquad Q_{2ij} = \frac{2\pi^4}{b^2}\left(\frac{B_iA_j}{l_il_j} - \frac{A_iB_j}{l_i^2}\right)Eh$$

$$T_{3ij} = -\frac{2\pi^4}{b^2}\left(\frac{B_iA_j}{l_il_j} + \frac{B_iA_j}{l_i^2}\right)Eh \qquad Q_{3ij} = \frac{2\pi^4}{b^2}\left(\frac{B_iA_j}{l_il_j} - \frac{B_iA_j}{l_i^2}\right)Eh$$

$$T_{4ij} = \frac{2\pi^4}{b^2}\left(\frac{A_iA_j}{l_il_j} - \frac{B_iB_j}{l_i^2}\right)Eh \qquad Q_{4ij} = \frac{-2\pi^4}{b^2}\left(\frac{A_iA_j}{l_il_j} + \frac{B_iB_j}{l_i^2}\right)Eh$$

$$\bar{N}_x = \sum_i Eh\,\frac{\pi^2}{2}\left[\frac{A_i^2}{l_i^2} + \frac{B_i^2}{l_i^2} + \frac{\nu}{4b^2}\left(A_i^2+B_i^2\right)\right] \Big/ (1-\nu^2)$$

$$\bar{N}_y = \sum_i Eh\,\frac{\pi^2}{2}\left[\frac{A_i^2+B_i^2}{4b^2} + \nu\left(\frac{A_i^2}{l_i^2} + \frac{B_i^2}{l_i^2}\right)\right] \Big/ (1-\nu^2)$$

$$\bar{N}_{xy} = 0$$

Performing the integration over the panel width and $n\ell/2$ wavelengths and letting n go to infinity, the equations of motion become:

$$\rho_m h \frac{\partial^2 A_m}{\partial t^2} = -\frac{\alpha_m}{b}\lambda B_m - \sqrt{\lambda\mu}\frac{\partial A_m}{\partial t} - A_m\left(\alpha_m^2 \bar{N}_x + \frac{\pi^2}{b^2}\bar{N}_y\right) + \sum_i \sum_j \sum_{\ell=1}^{4}\left(A^c_{\ell ijm} C_{\ell ij} + A^s_{\ell ijm} S_{\ell ij}\right)$$

$$\rho_m h \frac{\partial^2 B_m}{\partial t^2} = \frac{\alpha_m}{b}\lambda A_m - \sqrt{\lambda\mu}\frac{\partial B_m}{\partial t} - B_m\left(\alpha_m^2 \bar{N}_x + \frac{\pi^2}{b^2}\bar{N}_y\right) + \sum_i \sum_j \sum_{\ell=1}^{4}\left(B^c_{\ell ijm} C_{\ell ij} + B^s_{\ell ijm} S_{\ell ij}\right)$$

Where

$$A^c_{1ijm} = \sum_k \frac{\pi^2}{2b^2}\left(A_k\alpha_k^2 F(\ ) + \alpha_i\alpha_k A_k\left[F(jk) - F(ik)\right] - \frac{A_k}{4}\left[R_4 F(ij) - R_3 F(\ )\right]\right)$$

$$A^c_{4ijm} = \sum_k \frac{\pi^2}{2b^2}\left(A_k\alpha_k^2 F(ij) + \alpha_j\alpha_k A_k\left[F(ik) - F(jk)\right] - \frac{A_k}{4}\left[R_4 F(\ ) - R_3 F(ij)\right]\right)$$

$$A^c_{2ijm} = \sum_k \frac{\pi^2}{2b^2}\left(B_k\alpha_k^2 F(jk) - \alpha_k B_k\left[\alpha_j F(\ ) - \alpha_i F(ij)\right] + \frac{B_k}{4}\left[R_4 F(ik) + R_3 F(jk)\right]\right)$$

$$A^c_{3ijm} = \sum_k \frac{\pi^2}{2b^2}\left(B_k\alpha_k^2 F(ik) - \alpha_k B_k\left[\alpha_i F(\ ) - \alpha_j F(ij)\right] + \frac{B_k}{4}\left[R_4 F(jk) + R_3 F(ik)\right]\right)$$

$$B^c_{1ijm} = \sum_k \frac{\pi^2}{2b^2}\left(B_k\alpha_k^2 F(km) - \alpha_i\alpha_k B_k\left[F(jm) - F(im)\right] - \frac{B_k}{4}\left[R_4 F(ijkm) - R_3 F(km)\right]\right)$$

$$B^c_{4ijm} = \sum_k \frac{\pi^2}{2b^2}\left(B_k\alpha_k^2 F(ijkm) - \alpha_j\alpha_k B_k\left[F(im) - F(jm)\right] - \frac{B_k}{4}\left[R_4 F(km) - R_3 F(ijkm)\right]\right)$$

$$B^c_{2ijm} = \sum_k \frac{\pi^2}{2b^2}\left(B_k\alpha_k^2 F(jm) + \alpha_k A_k\left[\alpha_j F(km) - \alpha_i F(ijkm)\right] + \frac{A_k}{4}\left[R_4 F(im) + R_3 F(jm)\right]\right)$$

$$B^c_{3ijm} = \sum_k \frac{\pi^2}{2b^2}\left(B_k\alpha_k^2 F(im) + \alpha_k A_k\left[\alpha_i F(km) - \alpha_j F(ijkm)\right] + \frac{A_k}{4}\left[R_4 F(jm) + R_3 F(im)\right]\right)$$

$$A^s_{1ijm} = -\frac{\pi^2}{4b^2}\sum_k A_k\left(R_4 F(ij) - R_3 F(\ )\right)$$

$$A^s_{4ijm} = -\frac{\pi^2}{4b^2}\sum_k A_k\left(R_4 F(\ ) - R_3 F(ij)\right)$$

$$A^5_{2ijm} = \frac{\pi^2}{4b^2} \sum_K B_K \left(R_4 F(ik) + R_3 F(jk) \right)$$

$$A^5_{3ijm} = \frac{\pi^2}{4b^2} \sum_K B_K \left(R_4 F(jk) + R_3 F(ik) \right)$$

$$B^5_{1ijm} = -\frac{\pi^2}{4b^2} B_K \left(R_4 F(ijkm) - R_3 F(km) \right)$$

$$B^5_{4ijm} = -\frac{\pi^2}{4b^2} B_K \left(R_4 F(km) - R_3 F(ijkm) \right)$$

$$B^5_{2ijm} = \frac{\pi^2}{4b^2} A_K \left(R_4 F(im) + R_3 F(jm) \right)$$

$$B^5_{3ijm} = \frac{\pi^2}{4b^2} A_K \left(R_4 F(jm) + R_3 F(im) \right)$$

The function F(arguments) is defined by

$$8 \int_{-\frac{n\ell}{2}}^{\frac{n\ell}{2}} \cos\alpha_i x \cos\alpha_j x \cos\alpha_k x \cos\alpha_m x \, dx$$

with the provision that each of the cosine functions whose argument is ~~a~~ associated with an argument of F is replaced with a sine function of the respective argument.

$$R_{3ij} = \alpha_i^2 + \alpha_j^2$$

$$R_{4ij} = 2\alpha_i\alpha_j$$

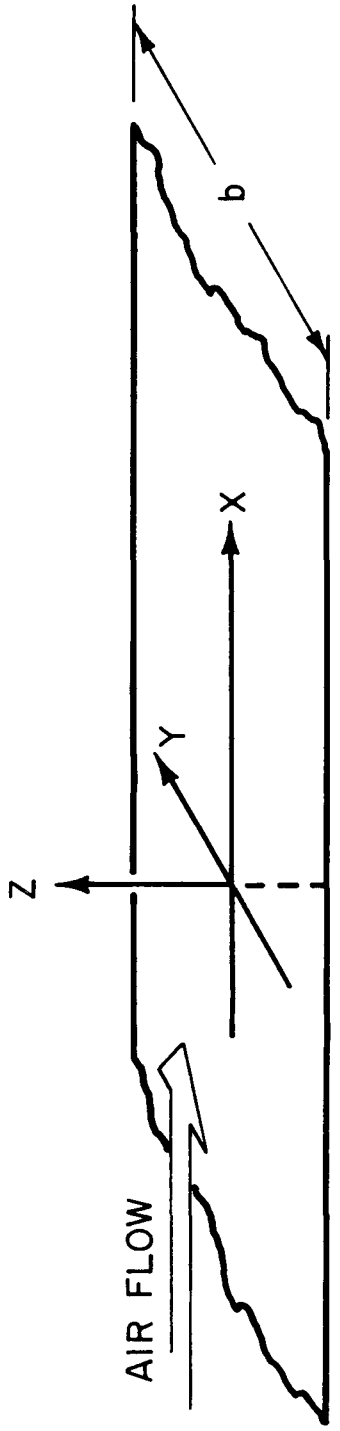

PLATE GEOMETRY

21

FIGURE 1

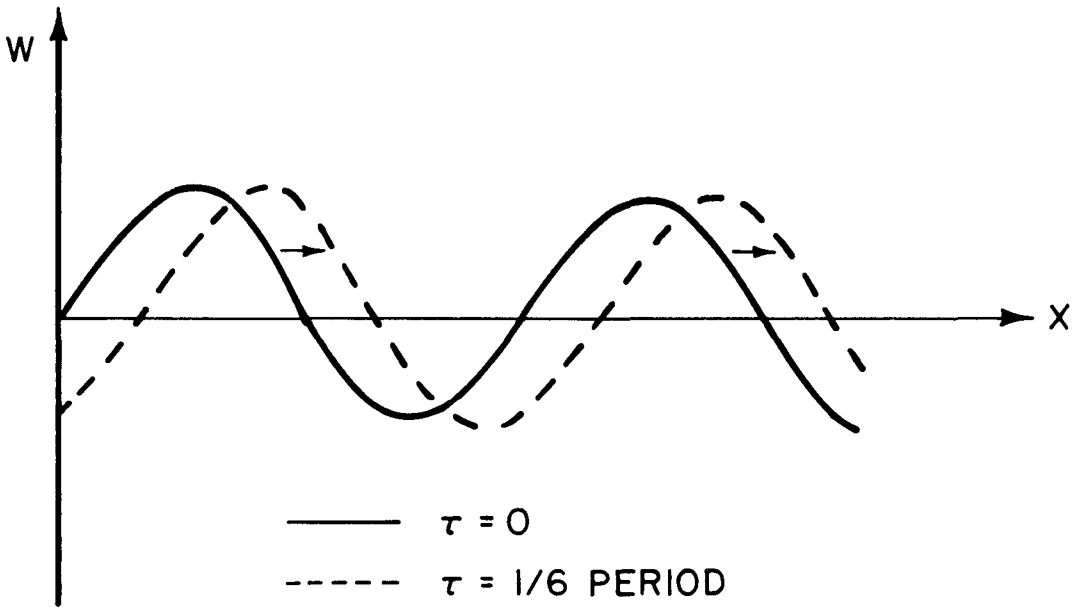

DEFLECTION SHAPE

38

FIGURE 2

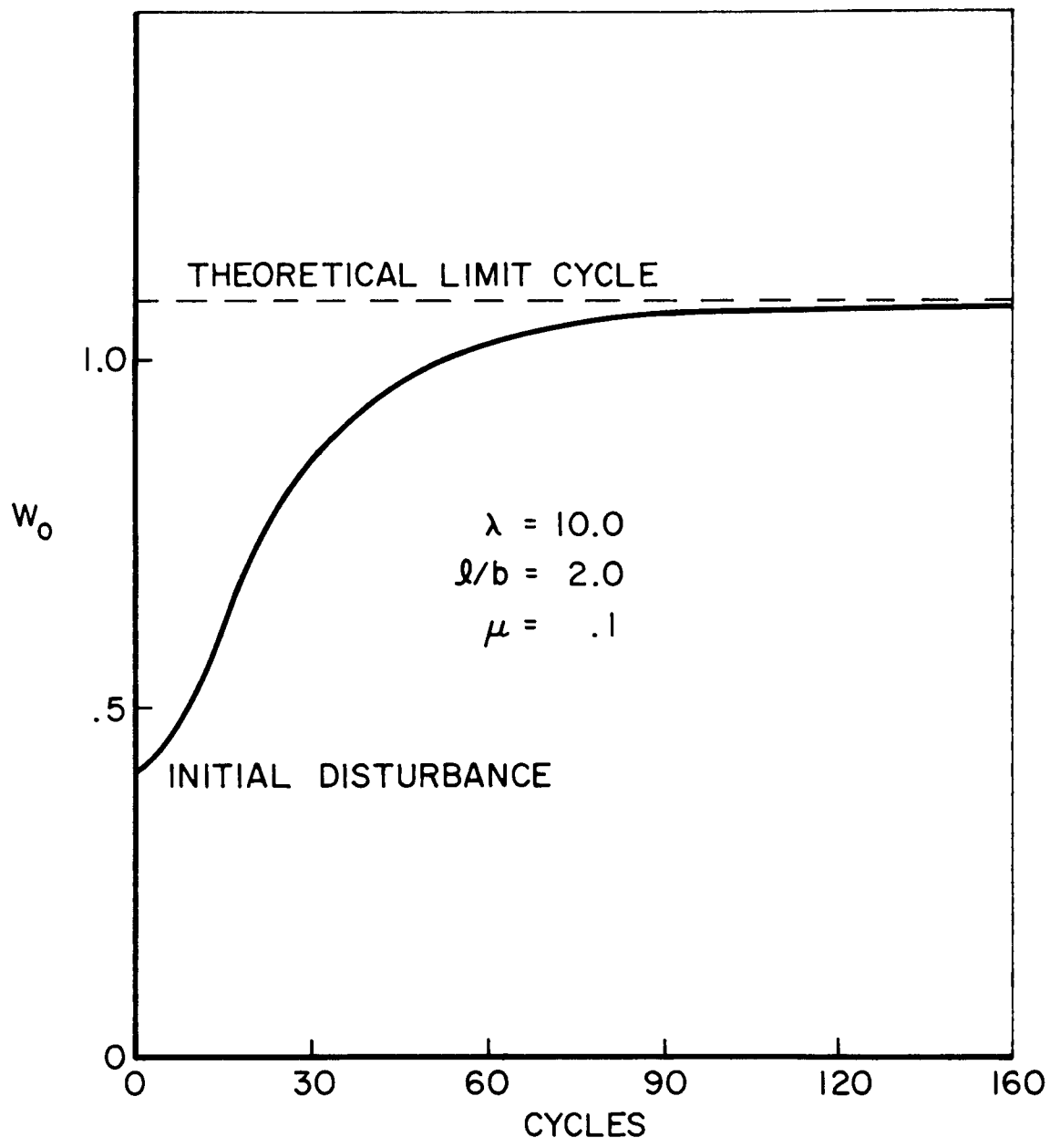

GROWTH OF A DISTURBANCE

FIGURE 3

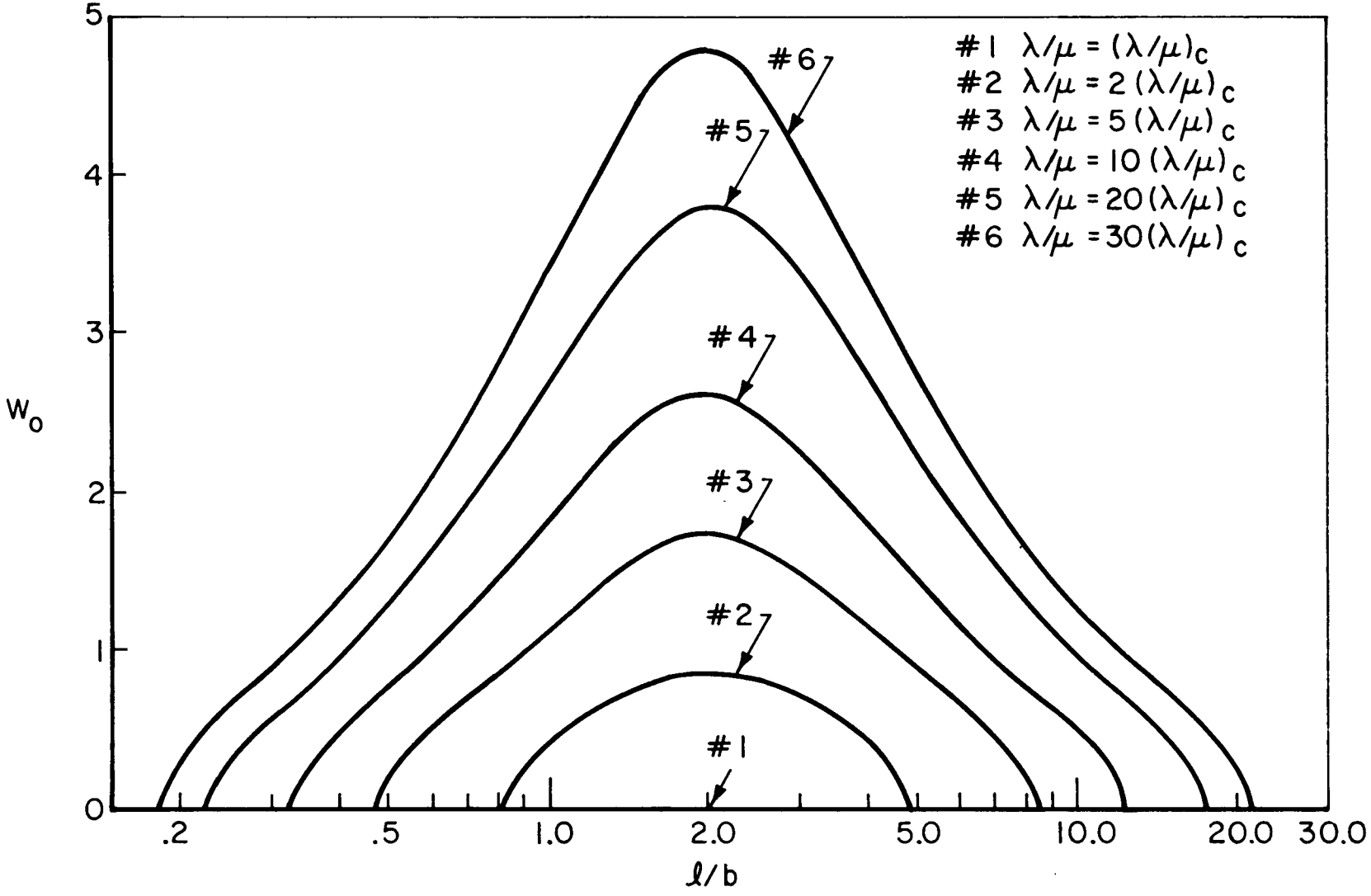

LIMIT CYCLE AMPLITUDE VS ℓ/b FOR VARIOUS λ/μ
DATA BOTH NUMERICAL ($\mu = .1$) AND ANALYTIC

FIGURE 4

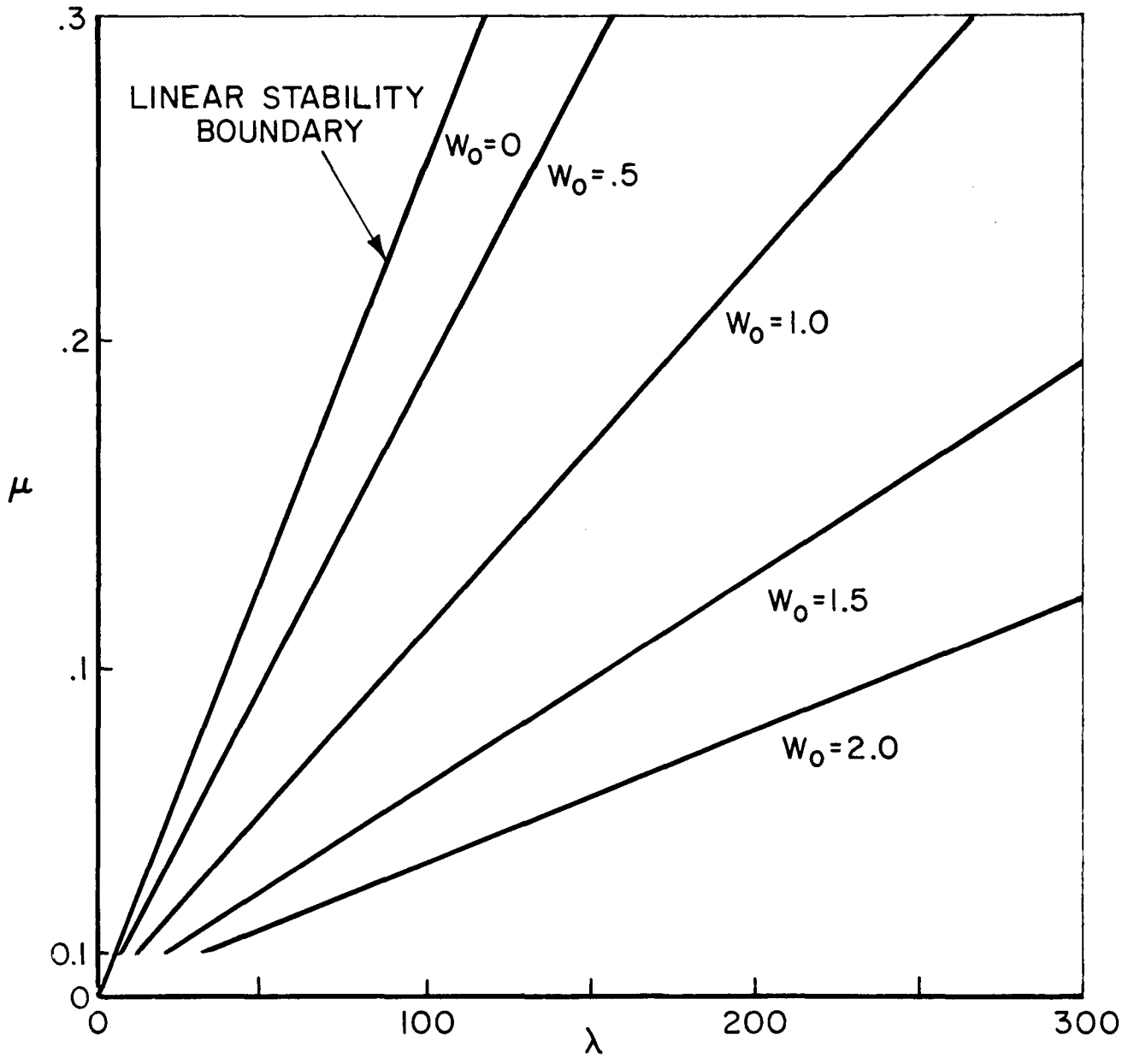

λ VS μ FOR VARIOUS LIMIT CYCLE AMPLITUDES, NUMERICAL DATA

FIGURE 5

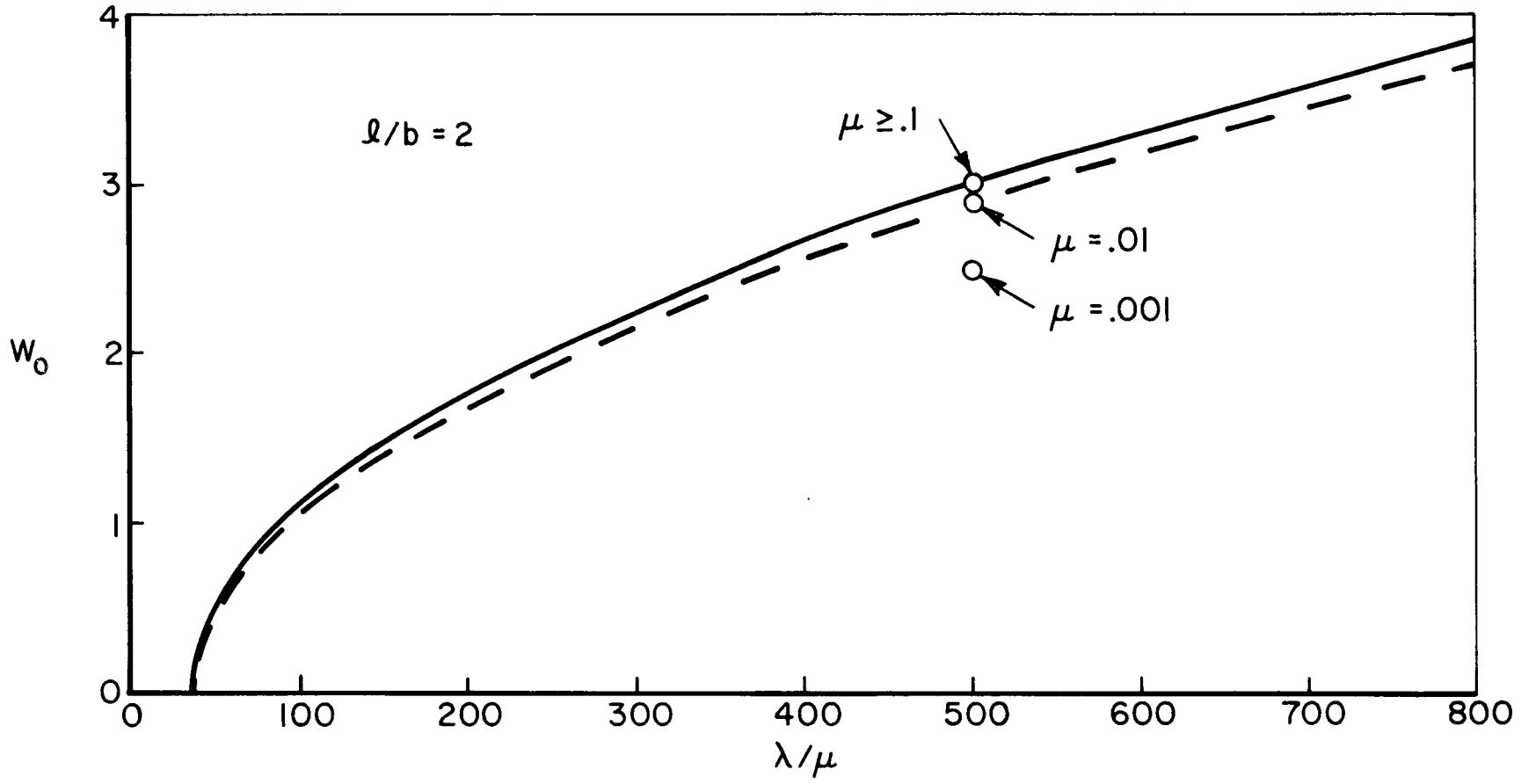

LIMIT CYCLE AMPLITUDE VS λ/μ, NUMERICAL RESULTS

32

FIGURE 6

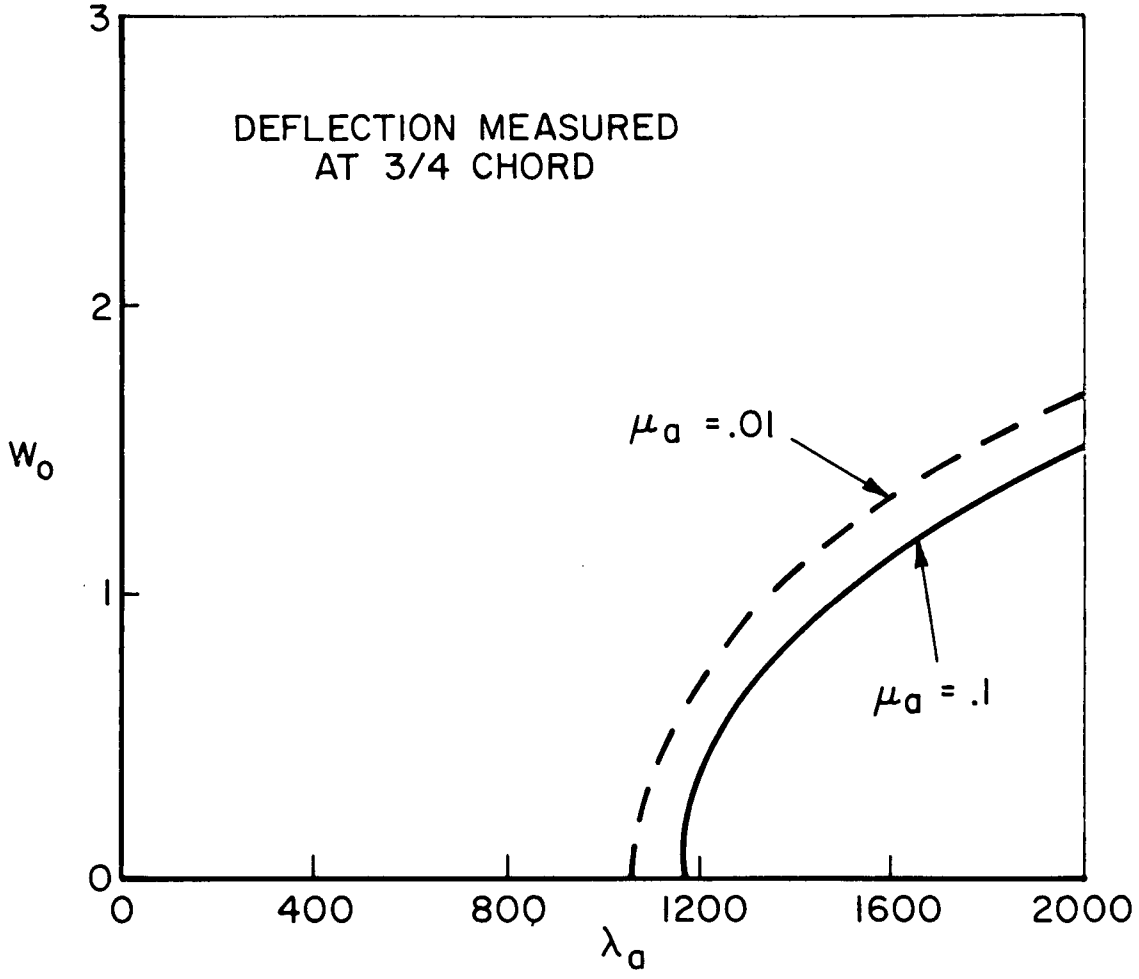

LIMIT CYCLE AMLITUDE VS DYNAMIC PRESSURE FOR FINITE PLATE WITH LENGTH TO WIDTH RATIO OF 2 (FROM FIGURE 16 IN DOWELL [4])

FIGURE 7

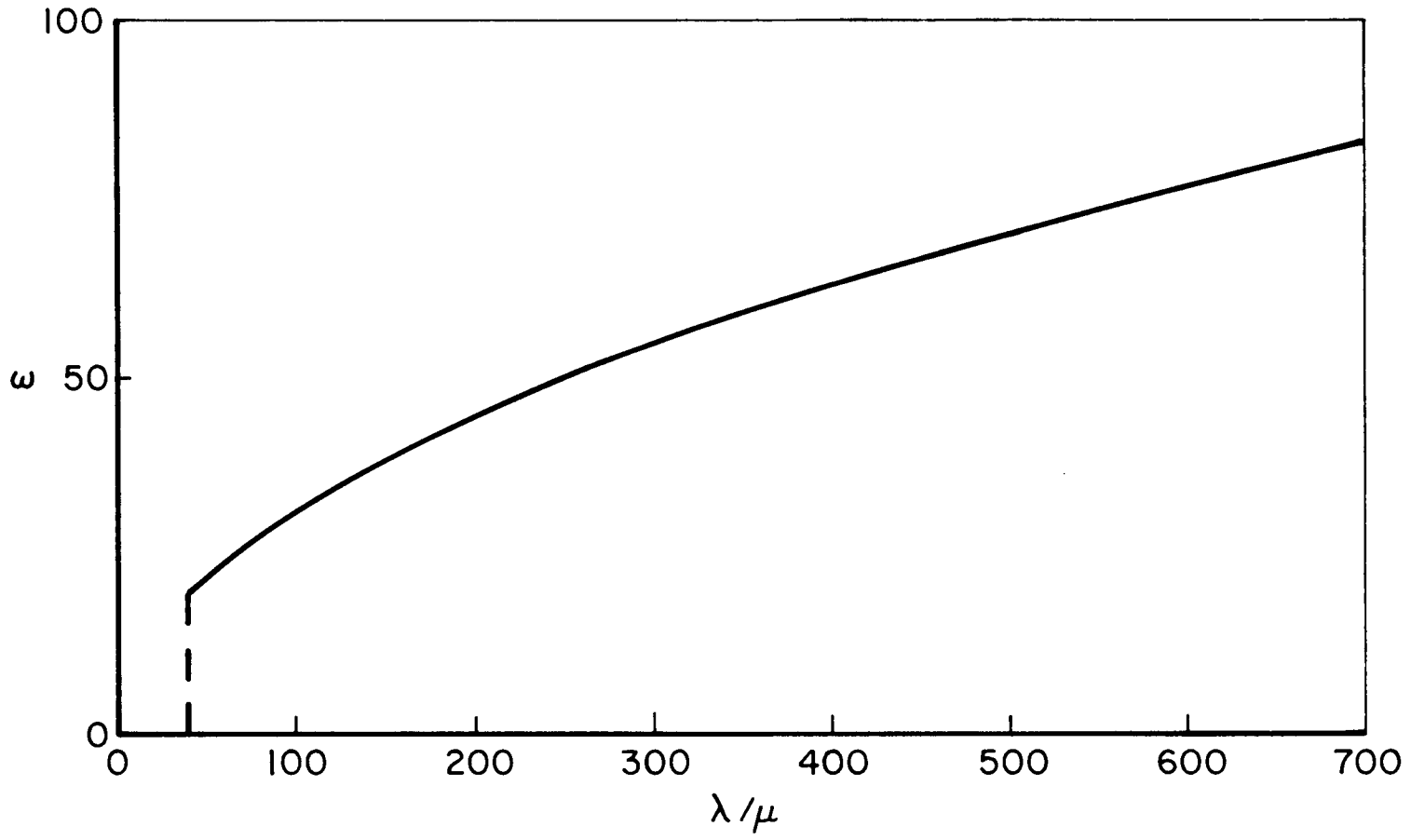

LIMIT CYCLE FREQUENCY AS A FUNCTION OF λ/μ, ANALYTIC DATA

34

FIGURE 8

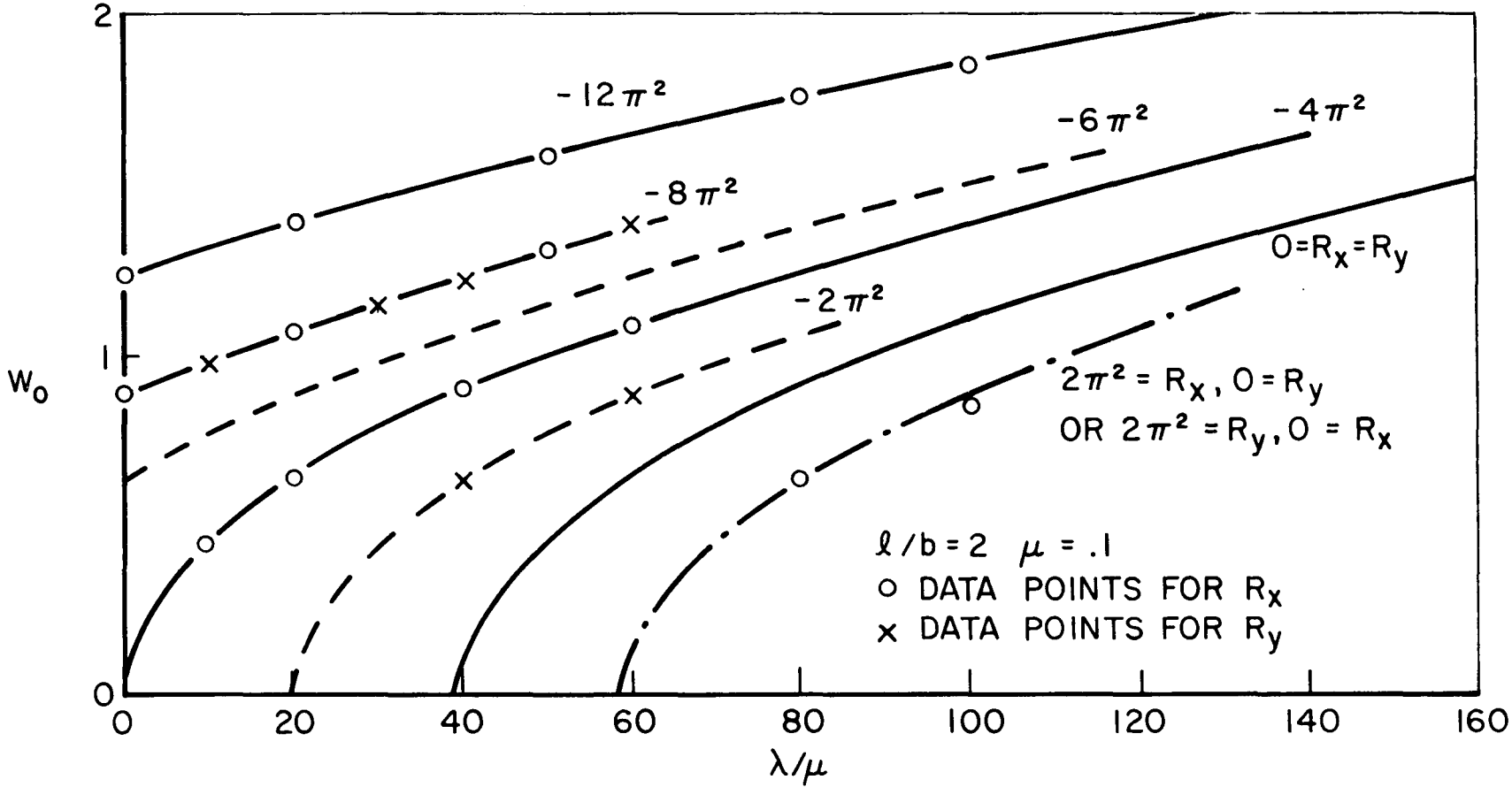

VARIATION OF LIMIT CYCLE AMPLITUDE WITH R_x AND R_y, ANALYTIC CURVES

FIGURE 9

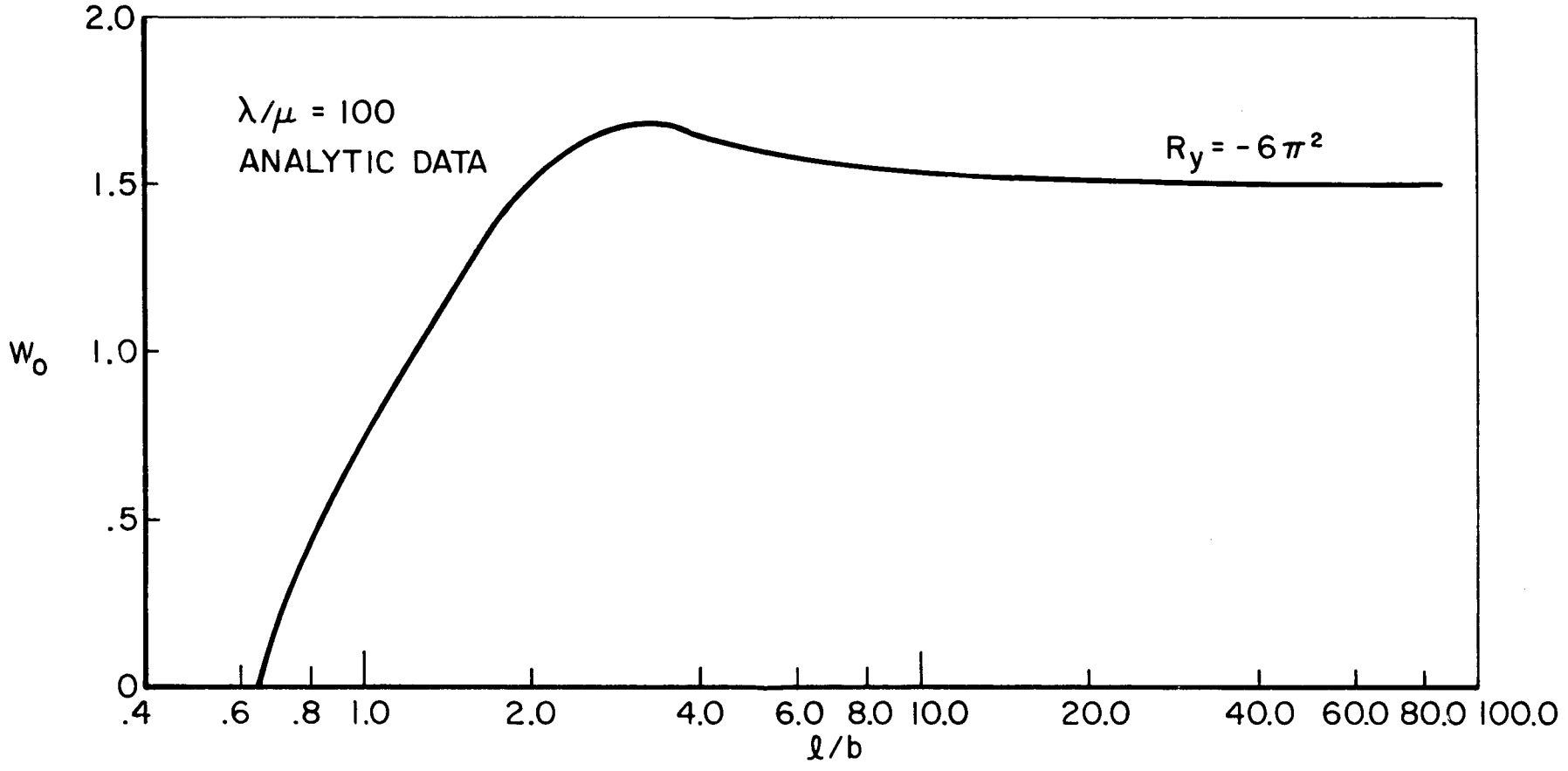

VARIATION OF DEFLECTION WITH ℓ/b
FOR PLATE COMPRESSED FROM THE SIDES

FIGURE 10

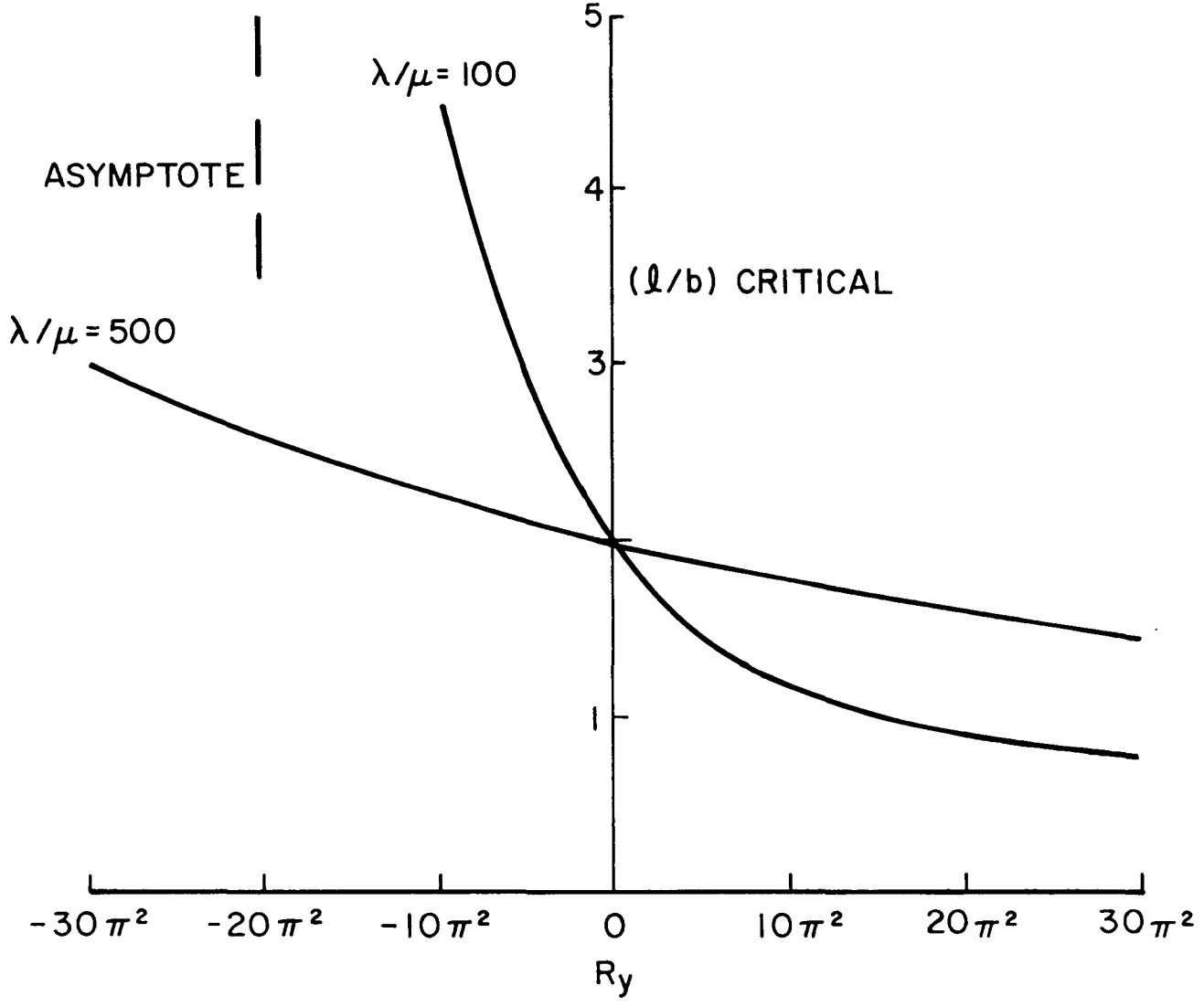

CRITICAL VALUE OF ℓ/b FOR R_y AND λ/μ, ANALYTIC DATA

FIGURE 11

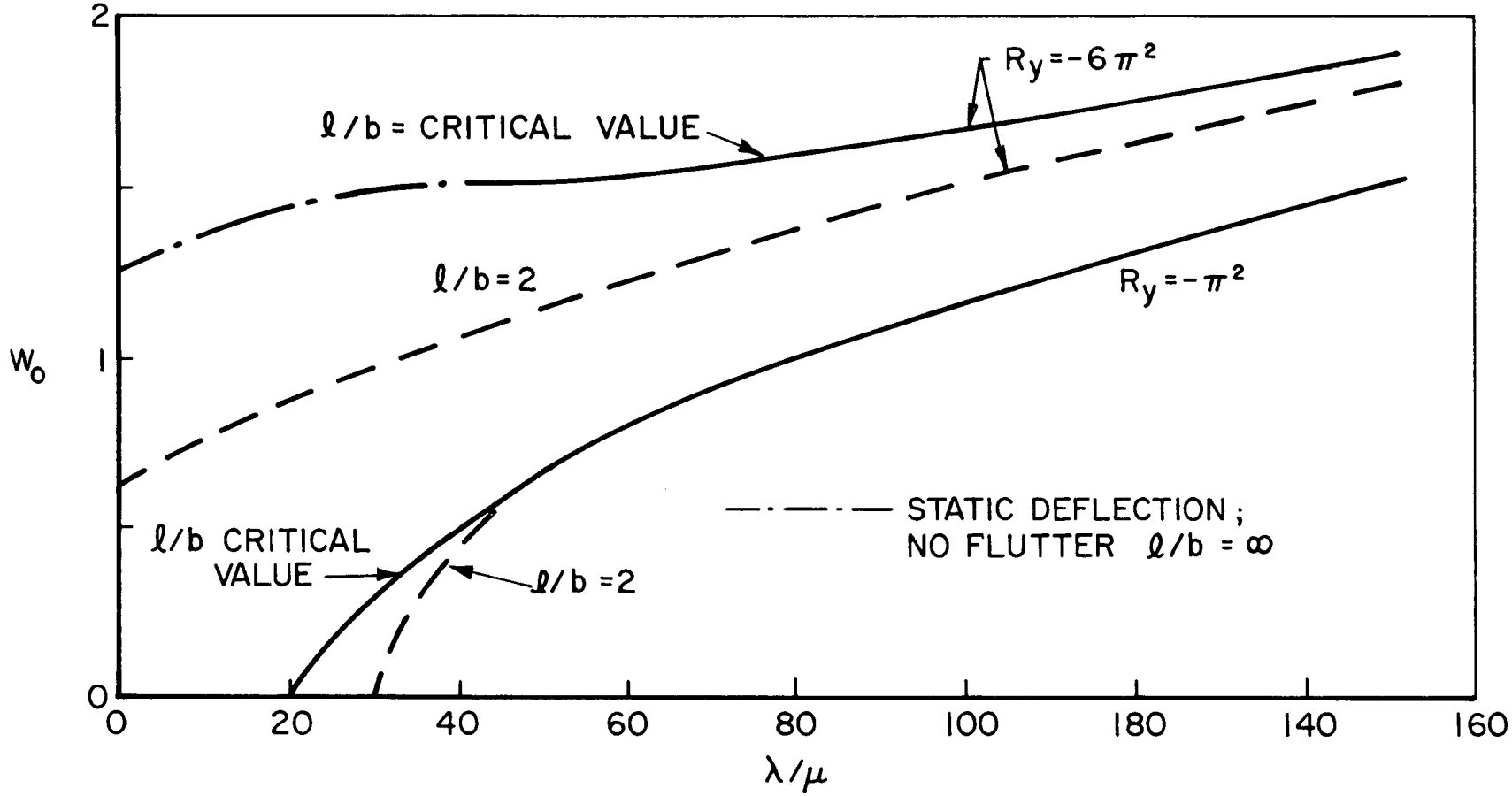

W_o FOR ℓ/b = CRITICAL VALUE COMPARED WITH $\ell/b = 2$, ANALYTIC DATA

FIGURE 12

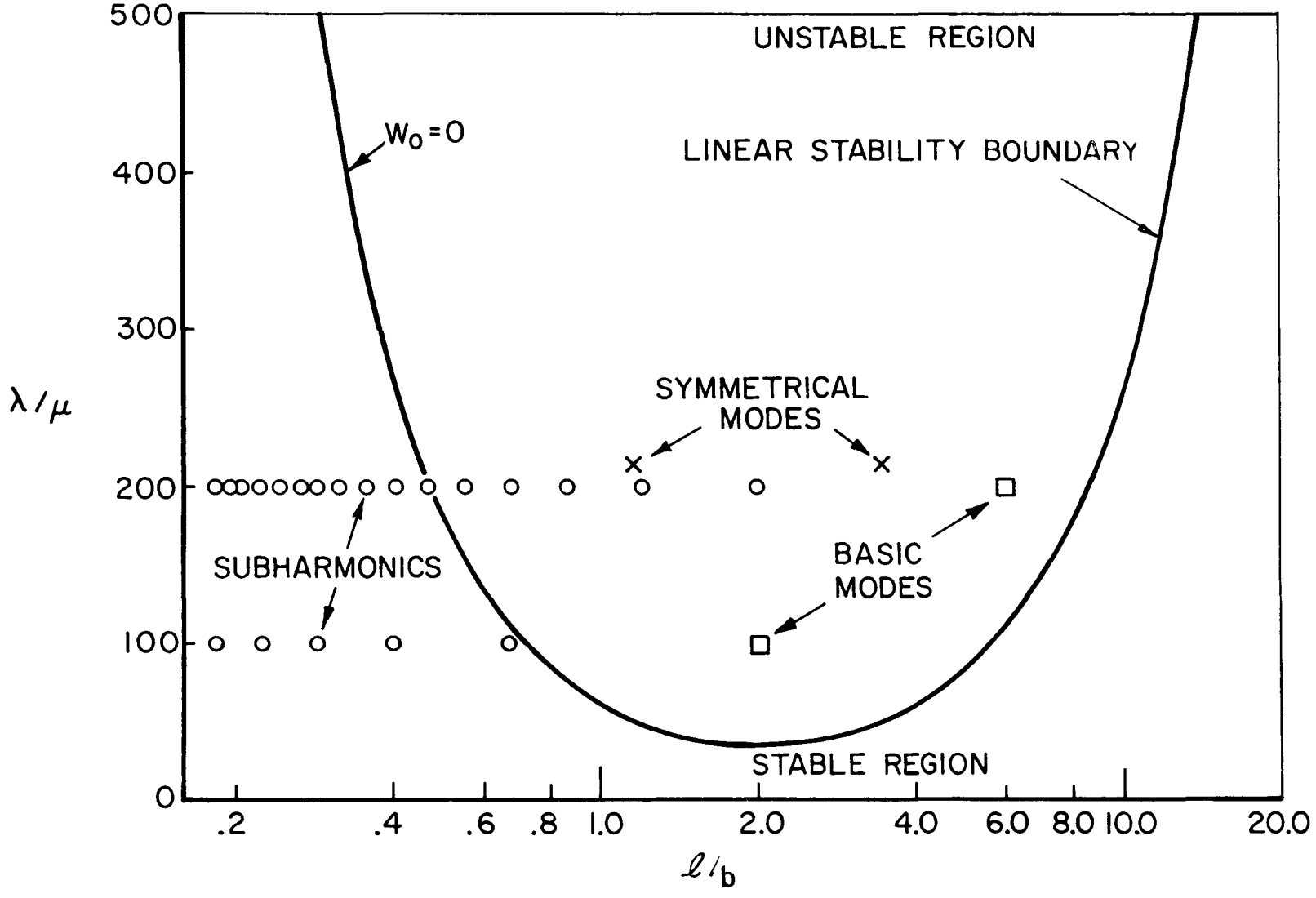

LOCATION OF MODES FOR MULTI-MODE SOLUTION

FIGURE 13